UNIVERSITY OF CALIFORNIA
RIVERSIDE

Seeded Growth of Silver Nanospheres and Their Self-Assembly Into Photonic Crystals

A Thesis submitted in partial satisfaction
of the requirements for the degree of

Master of Science

in

Materials Science and Engineering

by

Ze Chen

June 2022

Thesis Committee:
Dr. Yadong Yin, Chairperson
Dr. Ruoxue Yan
Dr. Juchen Guo

The Thesis of Ze Chen is approved:

Committee Chairperson

University of California, Riverside

Acknowledgement

Thank you for every number of the Yin group.

Special thanks to Dr. Yadong Yin, who supported me fully, tutored me in research, encouraged me when I lost my confidence, and told me not to give up. Many thanks to Qingsong Fan and Zuyang Ye, who answered many of my questions about academic research and life, and Zepeng Cai, who tutored me on this project. My appreciation also goes to those who helped me take TEM and SEM pictures, which was considerable work. Lastly, thank you all for supporting my research and graduate study!

Thanks to Dr. Juchen Guo and Dr. Ruoxue Yan, who supported me as thesis committee members and joined my final defense.

Thanks to Yin Lab, which gave me a platform to do experiments and provided expenditure, equipment, and chemicals for my Master's research. Thanks to UCR for giving me this excellent platform to study, do research, and furtherly let me learn more about myself.

Dedication

Thanks to my parents, who supported my living expenses during these periods and encouraged me to face all difficulties. They supported me and always encouraged me, helping me, again and again, to build up confidence.

ABSTRACT OF THE THESIS

Seeded Growth of Silver Nanospheres and Their Self-Assembly Into Photonic Crystals

by

Ze Chen

Master of Science, Graduate Program in Materials Science and Engineering
University of California, Riverside, June 2022
Dr. Yadong Yin, Chairperson

Silver nanostructures feature interesting optical properties due to their strong and tunable localized surface plasmon resonance. This paper studies the synthesis of silver nanospheres and their self-assembly into photonic crystals. Specifically, silver nanospheres are grown from seeds enclosed in uniform resorcinol-formaldehyde (RF) hollow nanoshells. The size and morphology of the silver nanoparticles can be controlled by the amount of silver precursor. The full-grown silver nanoparticles are near-spherical, with size determined by the RF templates, which can be controlled by starting with silica cores of defined diameters. The as-synthesized Ag@RF nanospheres can be assembled into colloidal photonic crystals to display bright diffractions at various wavelengths.

Table of content

List of figures

List of tables

1 Introduction

1.1 Optical properties of silver nanoparticles

Metal nanoparticles (NPs) have been used in many applications due to their unique optical properties arising from their interactions with incident light. Unlike nonmetallic materials, metal NPs have surface plasmon resonance (SPR). When a small metallic NP is irradiated by light, the oscillating electric field causes conduction electrons to oscillate coherently (Fig 1.1). When electrons are displaced relative to the nuclei, a restoring force that arises from Coulomb attraction between electrons and the nuclei results in the oscillation of electrons relative to the nuclear framework [1]. This property makes metal NPs attractive for a wide range of biomedical, energy, and information technologies applications.

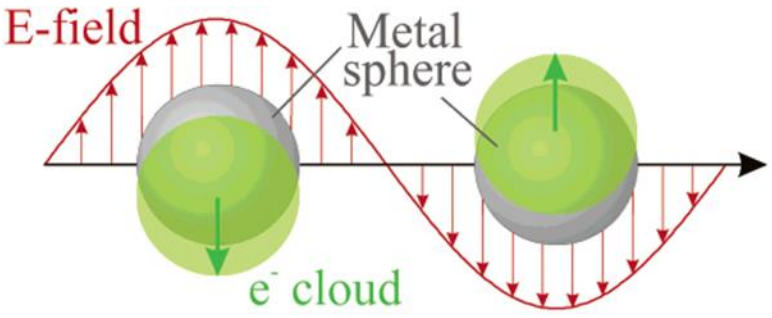

Fig 1.1 Schematic of plasmon oscillation for a sphere, showing the displacement of the conduction electron charge cloud relative to the nuclei [1].

As one type of noble metal, silver (Ag) has its unique optical properties because of SPR. From research by Mandelbaum et al. on numerical simulation of optical properties of Ag NPs based on Mei theory [2], compared with nonmetallic materials such as ZnO (4.2-1.2 from 300-1000 nm) [3] and SiO_2 (1.475 from 400-600nm) [4], the refractive index (RI) of Ag NPs was low in the visible region, but they have high extinction (Fig. 1.2a). Also,

the optical properties of Ag NPs vary according to their size. Paramelle et al. [5] researched the optical properties of Ag NPs with sizes from 8 to 100 nm. Fig. 1.2b shows that the extinction of Ag NPs increases with increasing NP size, and Fig. 1.2c shows that the absorption wavelength of Ag NPs increases with increasing NP size, but the absorption intensity decreases.

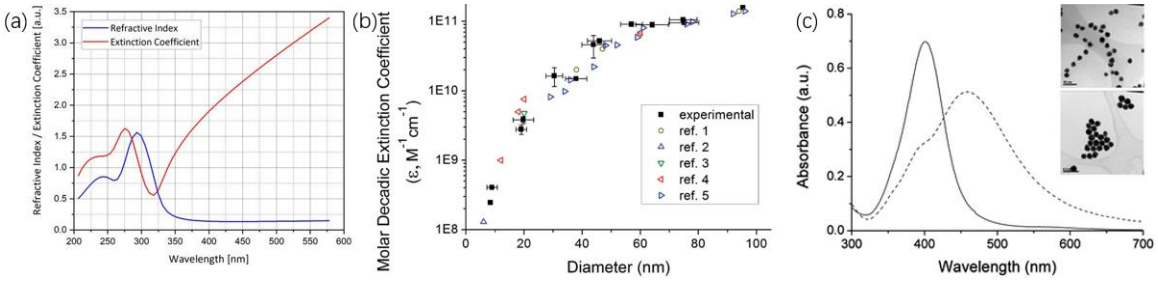

Fig. 1.2 a. Analytical model of Ag NP's RI and extinction coefficient according to Mie theory [2]. b. Comparison of molar decadic extinction coefficients at an absorbance at λ_{max} of experimental and literature data [5]. c. UV-visible spectra and TEM images of 19.0 nm (solid line and upper image) and 74.8 nm (dashed line and lower image) citrate-capped Ag NPs [5].

The contribution of the scattering to the extinction also changes with the size of Ag NPs. From the research of Evanoff and Chumanov [6] on extinction, scattering, and absorption cross-sections and efficiencies of Ag NPs with different sizes, Fig. 1.3 shows that for Ag NPs with a size around 30nm, extinction is dominated almost entirely by absorption. With increasing NP size, the fraction of scattering in extinction increased and then exceeded that of absorption.

In SPR, Ag is probably the most important material. Compared with other metal materials, Ag can provide a wider range of high SPR wavelengths, which is reflected in its higher quality factor Q (higher Q denotes less damping and a stronger plasmon resonance).

For the wavelength region in which Q > 10 for most plasmonic applications, Ag has a wavelength region of about 320-890 nm, which is wider than that of Au (about 640-820 nm) and Cu (about 620-680 nm) (Fig. 1.4a) [7]. Furthermore, Ag is relatively cheaper among these common SPR materials (Fig. 1.4b).

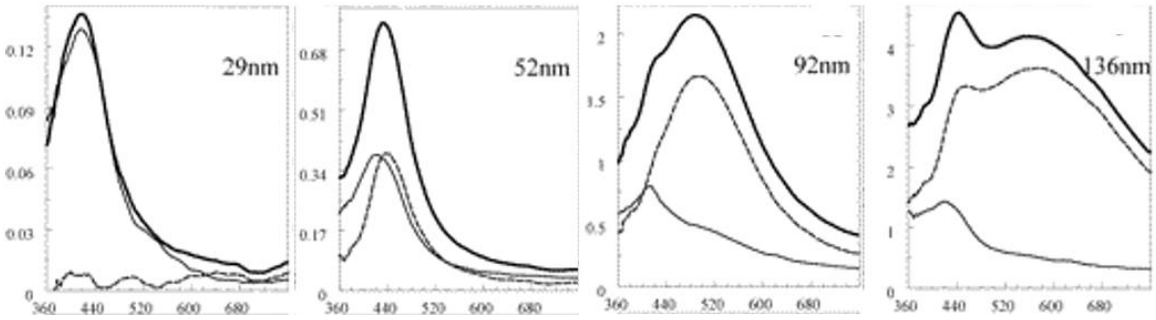

Fig. 1.3 Extinction (thick solid line), absorption (thin solid line), and scattering (dashed line) spectra of Ag NPs suspensions of different sizes normalized per single-particle [6].

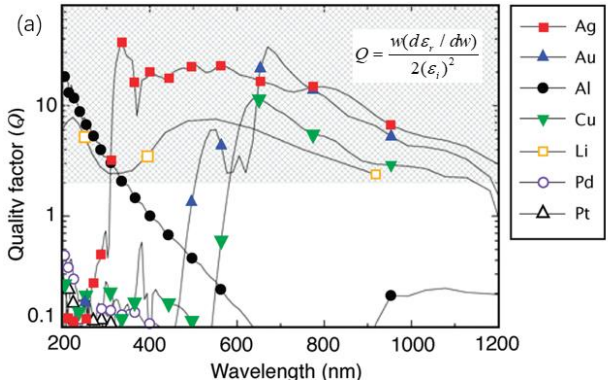

(b)

Materials	Price ($) /kg
Al	2.73
Cu	9.45
Au	59895
Pd	63514
Pt	32733
Ag	706

Fig. 1.4 a. Quality factor (Q) of the LSPR for a metal/air interface [7]. A higher Q denotes less damping and stronger plasmon resonance. The shaded area represents the region of interest for many plasmonic applications. b. Prices of common metal materials for plasmon resonance (*Prices on 06/04/2022).

1.2 Optical applications of silver nanoparticles

Due to the SPR and rich optical properties, Ag NPs have been used widely in optical applications. One direction is to use them for surface-enhanced Raman scattering (SERS).

Raman scattering is widely used to identify chemical species through specific interactions of light with matters. It is a light scattering technique in which molecules scatter incident light from a high-intensity laser light source. The laser light interacts with molecular vibrations, phonons, or other excitations in the system, resulting in the energy of the laser photons shifting up or down (inelastic collisions), which can provide information about both inorganic and organic chemical species. Although Raman scattering measurements provide a useful characterization of many materials, the signal is inherently weak (only about one in every million photons are inelastically scattered from the sample with energy different from the incident energy [8]), which restricts the usefulness of this analytical tool.

SERS is a technique in which inelastic light scattering by molecules is greatly enhanced when they are absorbed onto corrugated metal surfaces such as Ag or Au NPs [9]. For metal nanoparticles, localized SPR (LSPR) occurs when they are illuminated by incident light with the same wavelength as the electron resonance frequency, and electromagnetic enhancement occurs. At this condition, localized dipoles are created that enhance the localized electric field around the metal nanostructure (Fig. 1. 5). Molecules close to the higher electric field get stronger excitation, therefore, higher Raman signal. The other is chemical enhancement, which involves enhancement through a charge transfer mechanism between the substrate and the target molecule. Upon chemisorption of target molecules on the metallic substrate, new electronic states are formed, having possible intermediate energies resonating with the resonance frequency of the metal. Under

resonance, charge exchange occurs between the substrate and the molecule resulting in an enhancement in the Raman signal [8].

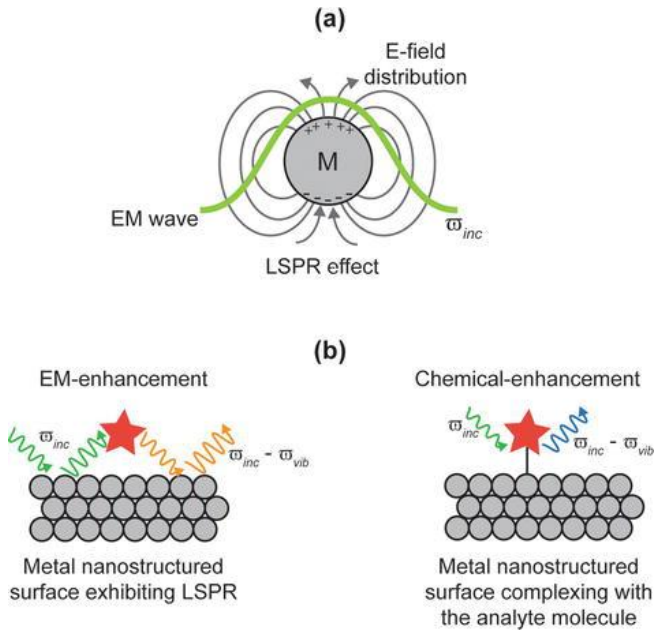

Fig. 1.5 a. Localized surface plasmon resonance (LSPR) effect exhibited by a metal NP in the presence of an electromagnetic wave with frequency ω_{inc} resonating with the plasmon frequency. b. SERS enhancement mechanism showing both electromagnetic (left) and chemical (right) enhancement of the scattering signal [8].

Zhong et al. [10] combined Ag NPs with porous silicon using an immersion plating solution to make photonic crystals as SERS substrate (Fig. 1.6a) for trace detection of picric acid (PA) and Rhodamine 6G dye (R6G). Compared with single-layer porous silicon, the enhancement factor (the intensity ratio between SERS and normal Raman scattering) of Ag-decorated porous silicon photonic crystals substrate increased by a factor of 3.58 at an R6G concentration of 10^{-6} mol/L, and there is still a valid signal even at a concentration as low as 10^{-10} mol/L (Fig. 1.6b). Also, it exhibited excellent sensitivity for the detection of PA as low as 10^{-7} mol/L (Fig. 1.6c).

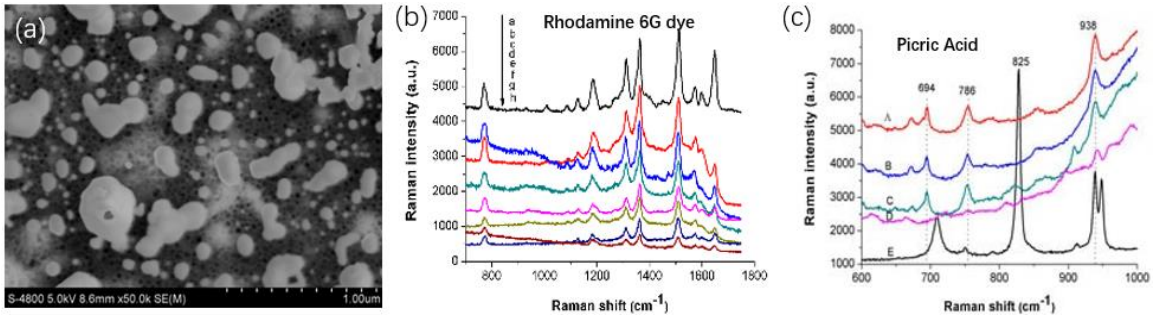

Fig. 1.6 a. Scanning electron microscope (SEM) image of PS/AgNPs photonic crystal substrates. b. SERS spectra of R6G in different concentrations from 10^{-3} to 10^{-10} mol/L (a to h). c. SERS spectra of PA in different concentrations from 10^{-4} to 10^{-7} mol/L (A to D) and solid PA (E) [10].

Hassan et al. [11] synthesized flower-like Ag NPs for rapid SERS sensing of pesticide residues: Methomyl, acetamiprid and 2,4-D in tea. The flower-like Ag NPs (Fig. 1.7a) were synthesized through the nucleation method without templates or seed solution, and the rough surface enhanced electromagnetic enhancement and provided a strong SERS effect. The SERS substrate synthesized by this kind of NPs has good detection for the above three pesticides (10^{-3} μg/L – 10^{3} μg/L for Methomyl, acetamiprid, and 10^{-2} μg/L – 10^{3} μg/L for 2,4-D) (Fig. 1.7b, c, d).

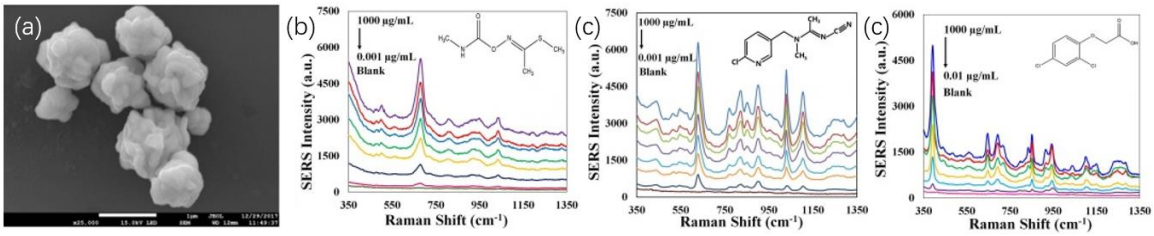

Fig. 1.7 a. SEM image of the flower-like Ag NPs and SERS spectra of b. methomyl, c. acetamiprid, and d.2,4-D in different concentrations [11].

Ag NPs can also be used in photonic crystals. Photonic crystals (PC) are a class of optical materials in which materials with different dielectric constants or RIs are

periodically organized in 1D, 2D, or 3D directions. According to Bloch's theorem, a photonic crystal has a bandgap and light with specific wavelengths cannot propagate in this structure. So, it can have selective inhibition or modulation of the propagation of light with specific wavelengths. Due to the low RI of Ag NPs in the visible region and the SPR effect, a PC containing tunable Ag NPs can change the RIs of its materials, which can further modulate its bandgap wavelength.

Yu et al. [12] found that with the transition between Ag and AgBr according to $2Ag + Br_2 \underset{UV}{\overset{Br_2}{\rightleftarrows}} 2AgBr$, 3D polystyrene (PS)/AgBr hybrid colloidal crystals (Fig. 1.8a) could be photosensitive and obtained noticeable structural color changes.

From Bragg's law of colloidal crystals used in this research, the maximum band gaps can be calculated from $k\lambda = 2\sqrt{2/3}D\sqrt{n^2 - \sin^2\theta}, k = 1, 2, 3.....$ where λ is the wavelength of the bandgap in the (111) direction, k is an arbitrary integer coefficient, D is the diameter of the colloids, n is the RI of the colloidal crystal, which $n^2 = \sum n_i^2 \times V_i$, and θ is the angle between incidence light and sample's normal. Because of the transition between the low RI of Ag NPs and the higher RI of AgBr (about 2.26), the RI of the total colloidal crystal could be changed, thereby further changing the bandgap wavelength λ.

Fig. 1.8b shows the color and color changes of PS/AgNPs colloidal particles exposed to different concentrations of Br_2 for 50 s. As the Br_2 concentration increased, the color changed from deep green to yellow, indicating the detection of Br_2.

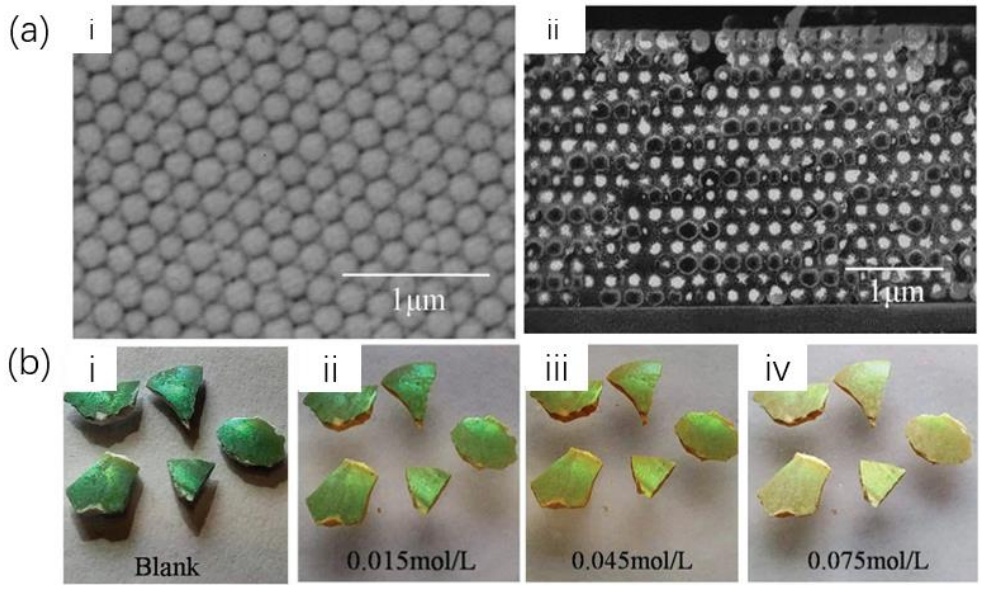

Fig. 1.8 a. SEM images of PS/AgBr hybrid colloidal crystals (front view (i) and section view (ii)). b. Photographs of the PS/AgNPs hybrid colloidal crystal sensor in contact with bromine gas of different concentrations for 50 s [12].

In the research of Aluicio-Sarduy et al. [13], they studied the tuning of the structural color, which is the active shift of the photonic bandgap, in a 1D photonic crystal made of alternating Ag NPs and TiO_2 NPs layers (Fig. 1.9a). A concomitant blue shift of the Ag plasmon peak and of the photonic bandgap of about 10 nm with a 10 V applied voltage was observed (Fig. 1.9c). They proposed the reason for this observation: the electric field induced the accumulation of polarization charges at the Ag/TiO_2 interfaces. These charges contribute to the plasma frequency of Ag and allow the electron density to increase over the entire volume of the Ag layer, resulting in an increase in the carrier density and a blue shift of the plasma frequency. Consequently, the effective RI of the whole photonic crystal was also changed, leading to the blue shift of the photonic bandgap.

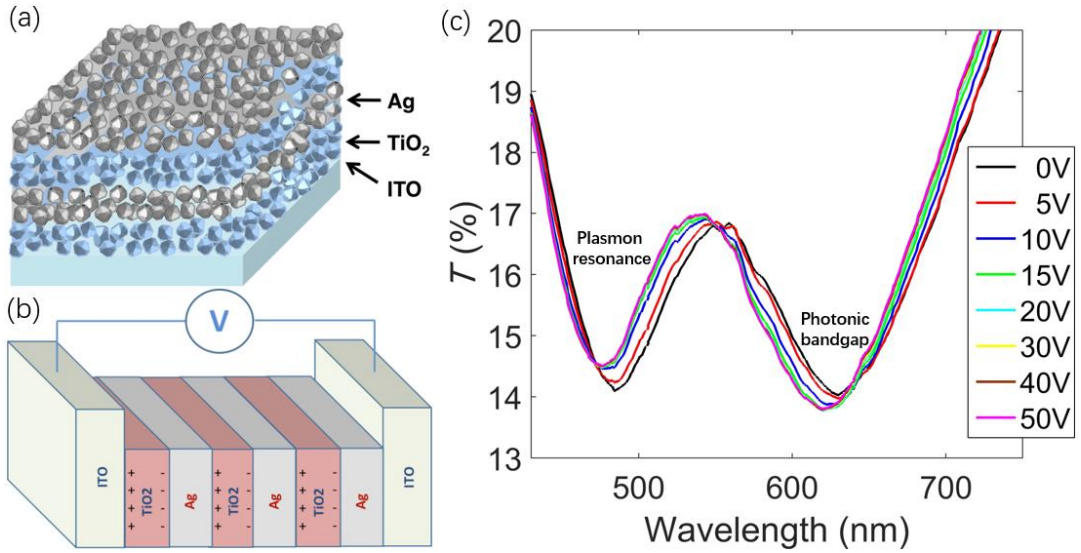

Fig. 1.9 a. Scheme of the one-dimensional photonic crystal made of layers of Ag NPs and TiO_2 NPs. b. Scheme of the interpretation of the action of the electric field on the indium tin oxide–(Ag-NP/TiO_2-NP)$_5$–Ag–indium tin oxide (ITO) photonic crystal device. c. Transmission spectra of the ITO–(Ag NP/TiO_2 NP)$_5$–Ag–ITO photonic crystal device upon application of an electric field [13].

The above two examples are PCs involving Ag NPs/Ag compounds with other nonmetallic materials. However, there are not many studies on using Ag NPs as the main material for PC, although there are cases of using self-assembled Ag NPs as a SERS substrate [14].

1.3 Research purpose and plan

This research aims to investigate the optical properties of photonic crystals using Ag@RF (resorcinol-formaldehyde) NPs as building blocks. The plan of this research is: first synthesize uniform Ag@RF NPs by the seeded growth method, in which the growth of Ag is achieved by adding different volumes of Ag^+ precursor. The Ag@RF NPs are then self-assembled on a piece of glass to form PCs. The relationship between the Ag growth condition and the optical properties of Ag NPs and corresponding PC will be investigated.

2 Materials and methods

2.1 Chemicals

Anhydrous ethanol is purchased from Decon Labs, Inc. Tetraethyl orthosilicate (TEOS, 99%), (3-aminopropyl)triethoxysilane (APTES, 99%), polyvinylpyrrolidone (mol wt 10000, 40000), tetrakis(hydroxymethyl)phosphonium chloride (THPC, 80% in H_2O), gold(III) chloride solution ($HAuCl_4$, 30wt% in dilute HCl), resorcinol (R, 99%), formaldehyde solution (F, 37 wt% in H_2O), L-ascorbic acid (AA, 99%) are purchased from Sigma-Aldrich, Co. Ammonium hydroxide ($NH_3{\cdot}H_2O$, 28-30 wt%), sodium hydroxide (NaOH, 97%), hydrofluoric acid (HF, 48-51% in H_2O), silver nitrate ($AgNO_3$, 99%), acetonitrile (ACN, 99%), ethylene glycol (EG, 99%) are purchased from Thermo Fisher Scientific, Co. Milli-Q water (H_2O for short) is from Milli-Q IQ water purification system.

2.2 Synthesis of silica (SiO_2) nanospheres

The synthesis of SiO_2 nanospheres with different sizes is controlled by using different concentrations of $NH_3{\cdot}H_2O$, with constant volumes of ethanol, TEOS, and water (Table. 1).

Ethanol (mL)	H_2O (mL)	TEOS (mL)	$NH_3{\cdot}H_2O$ (mL)
92	17.2	3.36	2.6
	17.9		1.9
	18.1		1.7
	18.3		1.5
	18.5		1.3

Table. 1 The volume of chemicals for synthesizing SiO_2 nanospheres of different sizes. The total volume of H_2O and $NH_3{\cdot}H_2O$ is 19.8 mL.

Add ethanol, water, and TEOS into a conical flask, stir with a speed of 600 rpm for 3min, and use a cylinder to inject $NH_3 \cdot H_2O$ quickly, seal the flask, and react for 4 h. Centrifugate the product (9000rpm 3min) and wash with ethanol twice and H_2O twice. Disperse the product into 40mL H_2O.

2.3 APTES modification of SiO_2 nanospheres

Wash 10mL of SiO_2 nanospheres with ethanol 3 times and is dispersed into 10 mL ethanol. The system of APTES modification is: 60 mL ethanol, 2.5 mL SiO_2 (in ethanol) in a three-neck flask, then stir and turn on circulating cooling water. After raising the temperature to 80 ℃, inject 2 mL APTES, keep the temperature for 3 h, let the system cools freely, and keep stirring for at least 12 h. The product is washed with ethanol 3 times and H_2O 2 times. The product is dispersed into 35 mL H_2O.

2.4 Synthesis of gold seeds

94.6 mL H_2O, 315 μl of NaOH aqueous solution (2 mol/L), and 126 μl THPC aqueous solution (5 times dilution) are added to a conical flask and stirred for 10min for pre-reaction. Then add 420 μl $HAuCl_4$ aqueous solution (0.25 mol/L) and stir for 5 min. Before use, store the product at 4 ℃ for 3 days.

2.5 Attachment of gold seeds and PVP modification of SiO_2 nanospheres

10 mL SiO_2@APTES NP aqueous solution is mixed with 10mL Au seed solution and stirred for 1 h. After separating the SiO_2 NPs by centrifugation, disperse the solution into 10 mL H_2O. For PVP modification, add 0.08 g PVP (mol wt 10000) into 5 mL H_2O and add 10 mL Au-seeds-attached SiO_2 nanosphere solution under ultrasonic dispersion.

The modification is overnight. Wash the product with H_2O twice and disperse it into 10mL H_2O.

2.6 RF coating and pre-treatment before silver growth

Add 21 mL H_2O, 2 mL R aqueous solution (10 mg/mL), 28 μl F, and 5 mL PVP-modified SiO_2 solution to a three-neck flask. After raising the temperature to 50 ℃, add 100 μl $NH_3 \cdot H_2O$ (2.8 wt%) and keep the temperature for 2 h. Then rise the temperature to 100 ℃ and keep it for 1 h. After the solution cools down, wash the product with H_2O twice and disperse it into 5 mL H_2O.

1 mL of 5% HF aqueous solution is added into1 mL of RF particle solution, and the mixture is treated with ultrasonic dispersion for 60 s. After washing with H_2O 3 times and dispersed into 1mL H_2O, add 1mL NaOH aqueous solution (0.1 mol/L), vibrate for 50 min, and wash with H_2O 3 times. Disperse the final product into 500 μl H_2O.

2.7 Silver growth

Add 1mL H_2O, 1mL PVP aqueous solution (mol wt 40000, 5 wt%), 1mL ACN, 100 μl AA aqueous solution (0.1 mol/L), 20 μl RF particle solution (after treatment) to glass bottle. The Ag^+ precursor is the mixture of $AgNO_3$ aqueous solution (10 mmol/L) and ACN ($V_{AgNO_3 solution} : V_{ACN} = 1:4$). Use an injection pump to inject the precursor into the growth solution at 5 μl/min rate. The product is washed with H_2O twice and dispersed into H_2O.

2.8 Self-assembly of Ag@RF nanoparticles

The Ag@RF NPs sample is washed with ethanol twice (add one drop of 2.8 wt% $NH_3 \cdot H_2O$ before the second wash to let nanoparticles take charge and pre-assemble). Abstract the remaining solution as much as possible, add 5 μl EG, and disperse. Clean the

glass with plasma cleaner for assembly. Use tape to create several small square areas (about 1 mm×1 mm) on glass and drop 1 μl of solution in one of these areas. Wait for the solution to spread out completely and put it into the oven and dry.

2.9 Characterizations

The SEM figures of SiO_2 nanospheres are characterized by TESCAN Vega3 SBH SEM. The size and polydispersity of SiO_2 NPs are characterized by the Desla™ Nano C Particle Analyzer. The TEM figures of the RF NPs before and after Ag growth are characterized by Thermo Scientific™ Talos L120C™ TEM. The UV-vis absorption spectra of the reaction solution in different stages are characterized by Ocean Optics HR2000 CG-UV-NIR spectrometer.

3 Basic mechanisms

3.1 Seeded growth method

The mechanism and advantages of seeded the growth method have been introduced in the article of Gao et al. [15]. In a typical seeded growth process of metal NPs, pre-formed metal NPs are employed as seeds, which are then incorporated into a growth solution composed of metal precursors and capping agents, etc., to initiate the growth of a secondary metal on the seeds.

Although the seeded growth method loses the convenience of the conventional one-step protocols for the synthesis of metal nanostructures, a great benefit that can be obtained from seeded growth is that a well-controlled growth step can be managed separately from the nucleation of the seeds so that sustained and predictable growth of the nanostructures

can be achieved. By controlling the concentration of the growth solution relative to that of the seeds and the growth time, it becomes possible to precisely control the size of the end product. Also in the seeded growth process, compared with a one-step synthesis in which high initial precursor concentration may cause self-nucleation, the concentration of the precursor in the growth solution can be well controlled to avoid additional nucleation so that newly reduced metal species can all be deposited onto the seeds and therefore result in continuous growth.

Therefore, the seeded growth method has been widely used as a versatile tool for rational design and synthesis of metal nanostructures of various compositions, structures, and morphologies, aiming at rendering the nanostructures with diverse functionalities for a broad range of applications including catalysis, imaging, and sensing.

3.2 Origin of the synthesis process

The synthesis method originates from the research of Chen et al. [16]. Fig. 3.1 shows the process. In their research, to realize the plasmonic coupling of several small Ag NPs, the seeded growth method was used to prepare plasmonic Ag nanostructures within confined spaces to achieve well-distributed interparticle distance for random plasmonic coupling. First, uniform ellipsoidal iron oxyhydroxide (FeOOH) nanorods were prepared as inner templates. Then, small Au seeds were synthesized and attached to the FeOOH templates' surfaces after FeOOH was premodified with polyethylenimine (PEI), which bound strongly to both and served as an effective bridging layer. As shown in Fig. 3.1a, Au seeds were randomly attached to FeOOH templates. To create tubular spaces, resorcinol-formaldehyde (RF) layers with suitable thickness were coated outside FeOOH

templates. After using oxalic acid for etching inner FeOOH templates and making hollow structures, rodlike RF nanotubes were obtained with Au seeds decorated on the inner walls.

When the reduction of Ag^+ was initiated with the help of AA, a significant number of metal atoms formed rapidly. These newly formed Ag atoms either deposit on the existing seeds or nucleate by themselves to eventually form free AgNPs. In this case, the chance of self-nucleation was high as the RF shell hinders the diffusion of Ag^+ ions to the inner part of the polymer shell. In order to prevent self-nucleation, the reduction potential of the Ag^+ precursor was reduced by complexing it with ACN and further decreased the reaction rate by slowly pumping the complex solution into the reaction system. Also, RF layers became porous upon pretreating with NaOH aqueous solution so that Ag^+ could enter to the inner space easier and reduce self-nucleation outside RF NPs.

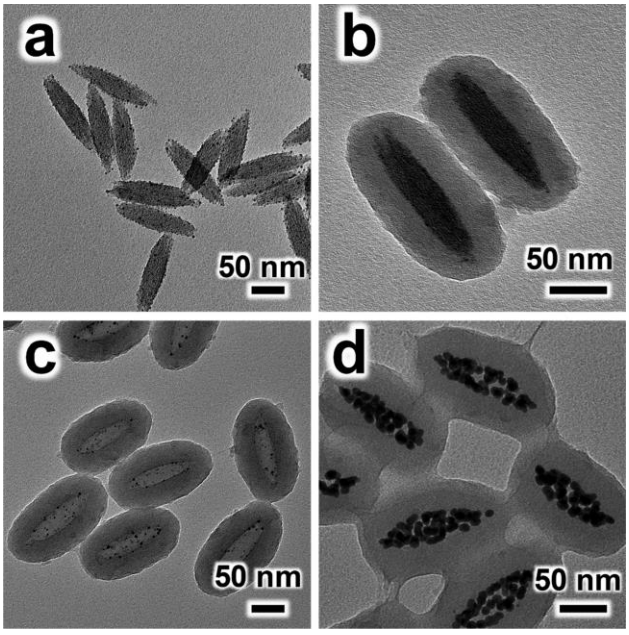

Fig. 3.1 TEM images of a. FeOOH nanorods with surface modified with Au seeds; b. FeOOH/Au nanorods overcoated with RF layers; c. hollow RF nanorods containing Au seeds on the inner surface prepared by removing FeOOH; d. RF nanorods with Ag NPs assemblages upon the growth of Ag on Au seeds [16].

3.3 Mechanism of SiO_2 nanospheres synthesis

The synthesis of uniform SiO_2 templates is carried out by the Stöber method. It is ammonia-catalyzed sol-gel reaction hydrolysis of TEOS that occurs in the presence of water and low molecular weight alcohols like ethanol, followed by subsequent condensation [17].

3.3.1 Sol-gel process

Sol is a phase in which colloid particles disperse and suspend in liquid. The size of particles is 1-100nm. Gel is a semi-solid material, which is full of liquid after sol loses fluidity. Solid particles will be in a continuous net structure. The phases of sol and gel have a relationship which is the condensation process of sol particles becoming chain. In this sol-gel process, SiO_2 will be composed of silane, which first hydrolyzes, becomes intermediate, followed by progressive condensation, and becomes a 3D network. The motion of intermediate molecules is limited, and the system can produce a gel with a uniform phase. Chemical reactions involved in forming SiO_2 NPs are hydrolysis of TEOS and condensation.

3.3.2 Hydrolysis of TEOS

The primary reaction during the Stöber synthesis is the hydrolysis of TEOS, the most common SiO_2 precursor. It involves the nucleophilic substitution of ethoxy groups (-Si-OR) by silanol groups (-Si-OH) via a penta-complexation transition state. In general, hydrolysis occurs in the presence of water, but it can be efficiently catalyzed with acid or base. In the typical Stöber synthesis, $NH_3 \cdot H_2O$ is used as a catalyst to accelerate the rate of hydrolysis and condensation. The OH^- present in $NH_3 \cdot H_2O$ solution is more effective

nucleophiles compared to H_2O molecules. Fig. 3.2a shows the entire process of TEOS hydrolysis, in which the reaction equation is: $Si(OC_2H_5)_4 + 4H_2O \rightarrow Si(OH)_4 + 4C_2H_5OH$. The first hydrolysis step is slower and is a rate-determining step. However, the rate increases as more silanol groups are converted to ethoxy groups due to the increased positive charge of silicon atoms and reduced steric hindrance by replacing ethoxy groups with OH^- nucleophiles.

3.3.3 Condensation

Fig. 3.2b shows the condensation process. Hydrolysis is followed by condensation, where silanol groups (-Si-OH) of SiO_2 monomers or oligomers condense to form siloxane (Si-O-Si) bonds. Like hydrolysis reaction, it involves the nucleophilic substitution reaction. But the rate of condensation is much faster than hydrolysis, as the silanol groups are deprotonated more easily than water molecules to increase positive charge density on silicon atom to make a favorable nucleophilic attack.

3.3.4 Nucleation and growth

After the hydrolysis and condensation process, there are precursors in the solution. When its concentration is up to a certain level, nucleation will happen. From La Mer and Dineger's research [18] on the monomer addition model in 1950 about the nucleation and growth of sulfur, it is found that the growth of SiO_2 NPs in the sol-gel process is similar (Fig. 3.3a). Fig. 3.3b shows that when the concentration of formed monomers increases and exceeds the critical supersaturation concentration C_s, and reaches C_{min}, it surpasses the activation barrier for self-nucleation and begins to nucleate. This process will continue until the concentration of monomers in the reaction system reduces below the nucleation

threshold. After this, new nuclei are barely formed, and the growth of the existing nuclei occurs by monomer addition with the preferential deposition of soluble monomers on the growing polymeric solid, become primary particles, and later be stable. Finally, colloidal particles are formed [17]. According to this model, uniformity and monodispersity are assured by the effective separation of nucleation and growth process.

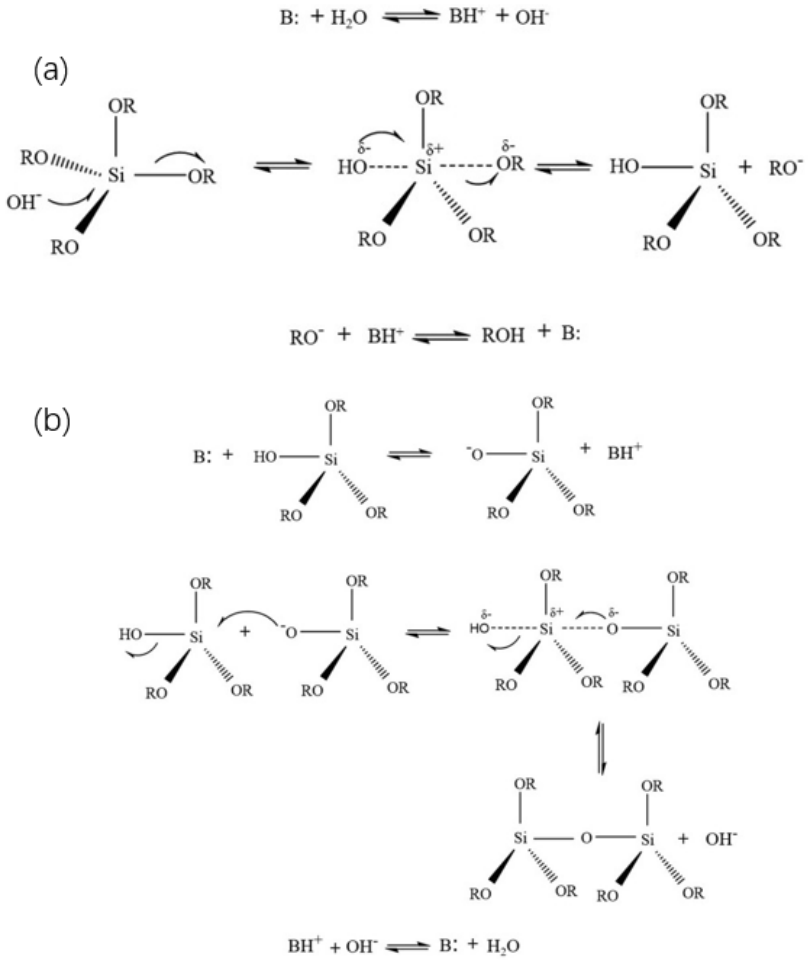

Fig. 3.2 Mechanisms of a. hydrolysis and b. condensation of TEOS precursors in base (B:)-catalyzed reactions [17].

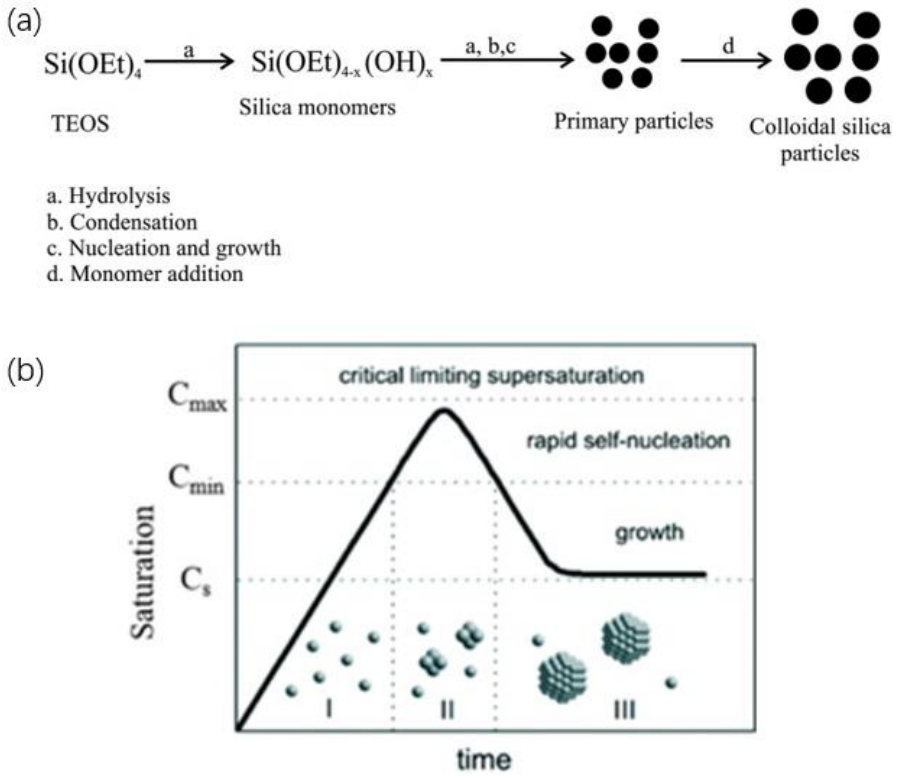

Fig. 3.3 Illustrations of a. monomer addition model during the formation of colloidal SiO_2 and b. Lamer and Dinegar's model of nucleation and growth [17].

3.4 Size control of SiO_2 nanospheres

The size of SiO_2 nanospheres can be controlled by varying the concentration of $NH_3 \cdot H_2O$, H_2O, TEOS, and the type of solvent [17].

3.4.1 Effect of $NH_3 \cdot H_2O$ concentration

$NH_3 \cdot H_2O$ acts as the catalyst in the hydrolysis of TEOS reaction. According to the reaction mechanism, higher $NH_3 \cdot H_2O$ concentration will enhance the degree of hydrolysis and condensation, leading to larger SiO_2 nanospheres. In contrast, when the concentration

of $NH_3 \cdot H_2O$ is low, the sizes of SiO_2 nanospheres are relatively smaller as less hydrolyzed monomers are produced. The research from Han et al. [19] shows that with increasing $NH_3 \cdot H_2O$ concentration in SiO_2 nanospheres synthesis in ethanol system (0.25, 0.50, 0.73, 0.95, 1.17, and 1.58 mol/L), the particle size increased to 16 nm, 62 nm, 162 nm, 350 nm, 415 nm, and 480 nm respectively (Fig. 3.4). However, compared with size increase, the polydispersity had the opposite trend: it decreased from 24.3%, 18.3%, 11.6%, 3.6%, and 4.3% in the respective samples.

The temporal evolutions of the particles at higher and lower $NH_3 \cdot H_2O$ concentrations are shown in Fig. 3.5 [19]. In the system with a lower $NH_3 \cdot H_2O$ concentration system (0.5M), the partially hydrolyzed silanol monomers $Si(OEt)_3(O^-)$ were formed, which upon condensation resulted in branched, aggregated siloxane clusters with fewer negative charges on the surface. Upon further hydrolysis and condensation, small, dense particles were formed. In contrast, TEOS hydrolysis at higher $NH_3 \cdot H_2O$ concentration (1.17 mol/L) led to more hydrolyzed silanol monomers, which not only aggregated into a highly-condensed structure but also exhibited more negative charge on the surface that repelled each other. Hence, the newly formed silanol monomers in the reaction medium were added instead of diffusing into the pre-formed siloxane network, increasing the size of colloidal particles.

From the research of Wang et al. [20], apart from the hydrolysis reaction rate, $NH_3 \cdot H_2O$ also controls the aggregation of SiO_2 particles. OH^- provided by $NH_3 \cdot H_2O$ transfer negative charges to the SiO_2 surface and developed electrostatic repulsion can

prohibit aggregation. But the study by van Blaaderen et al. [21] shows that too high a concentration of $NH_3 \cdot H_2O$ would decrease colloidal stability as the ionic strength is too high.

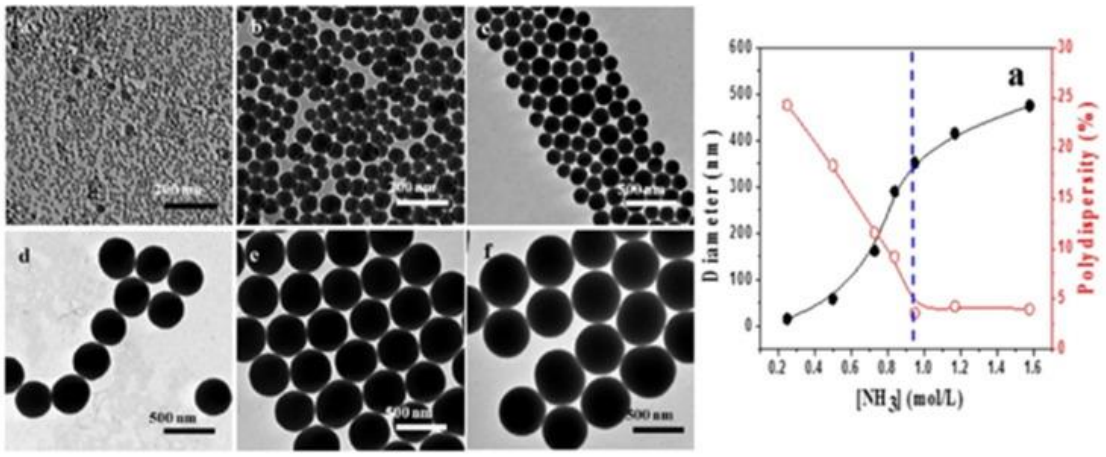

Fig. 3.4 TEM images of SiO_2 particles prepared at different $NH_3 \cdot H_2O$ concentrations: a. 0.25 mol/L, b. 0.50 mol/L, c. 0.73 mol/L, d. 0.95 mol/L, e. 1.17 mol/L and f. 1.58 mol/L, respectively; the effect of $NH_3 \cdot H_2O$ concentration on the size and polydispersity of SiO_2 particles [19].

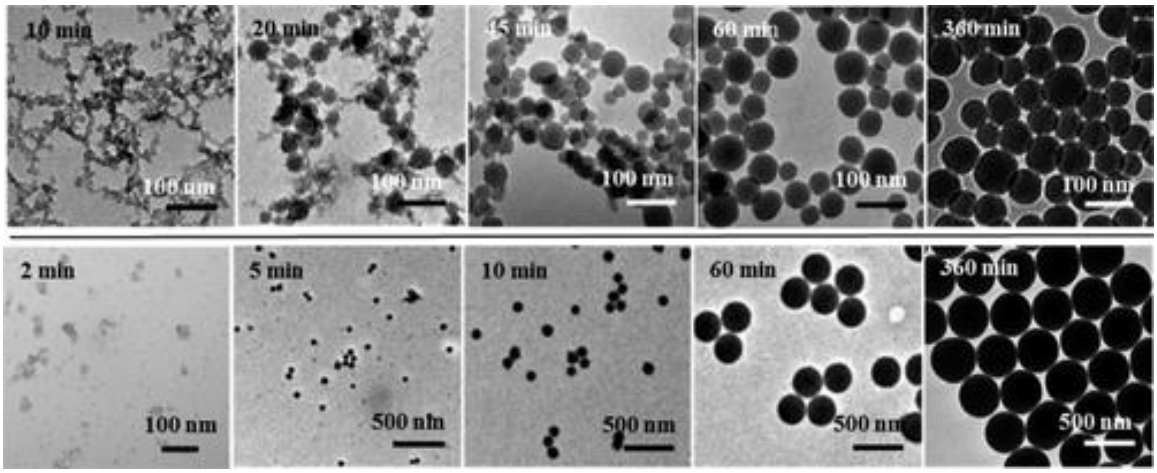

Fig. 3.5 TEM images of SiO_2 particles growing in the reaction solution at different $NH_3 \cdot H_2O$ concentrations of 0.5 mol/L (upper panel) and 1.17 mol/L (lower panel) via Stöber method [19].

3.4.2 Effect of TEOS concentration

Increasing TEOS's concentration will also raise the numbers of hydrolyzed monomers and finally increases the size of SiO_2 nanospheres. Yan et al. [22] researched the quantitative relationship between TEOS concentration and the size of SiO_2 nanospheres (Fig. 3.6). In the system in which co-solvent was methanol, when fixed water and $NH_3 \cdot H_2O$ concentration, the size of SiO_2 nanospheres had a good linear relationship with TEOS concentration (from 0.15 mol/L to 0.25 mol/L). And Wang et al. [20] found that too high a concentration of TEOS could cause agglomeration of SiO_2 particles.

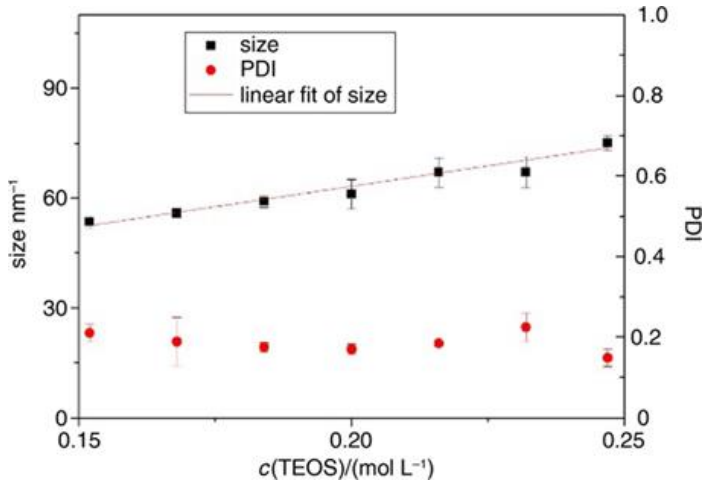

Fig. 3.6 Effect of TEOS concentration on the size and dispersion of SiO_2 NPs. Reaction conditions: ammonia concentration, 0.4 mol/L; water loading, 0.50 mL; methanol loading, 2.0 mL; room temperature; reaction time, 12 h [22].

3.4.3 Effect of water concentration

Increasing the water concentration can significantly increase the hydrolysis rate of TEOS as it can have a lower nucleation period and faster nucleation rate [23], causing larger particle sizes. Also, some research shows that increasing the water concentration can

increase the separation distance between monomers and affect the growth rate. And Park et al. [24] found that larger particles existed under high water concentration but were obtained by agglomeration of small primary particles (Fig. 3.7a). They explained this as a function of stronger H-bonding (at high H_2O content) that led to the coalescence of particles (Fig. 3.7b). Therefore, an optimum amount of water played a vital role in controlling the size of SiO_2 particles. For monodispersity, Yan et al. [22] show that with increasing water concentration, the polydispersity of SiO_2 NPs increased obviously (Fig. 3.7c).

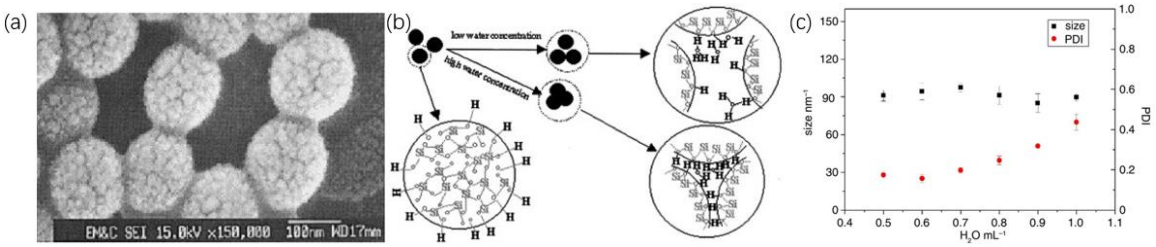

Fig. 3.7 a. SEM image of SiO_2 NPs obtained at high water concentration. b. Effect of water concentration on the particle size and distribution [24]. c. Effect of the amount of water on the size and dispersion of SiO_2 NPs. Reaction conditions: TEOS concentration, 0.2 mol/L; ammonia concentration, 0.4 mol/L; methanol loading, 2.0 mL; room temperature; reaction time, 12 h [22].

3.4.4 Effect of solvent type

Fig. 3.8 shows the increase in the size of SiO_2 nanospheres as the type of alcohol changes from methanol to n-butanol. Although the reason for the increased size is unclear, Bari et al. [25] indicated that the increase in viscosity and decrease in polarity of long-chain alcohols could make SiO_2 nanospheres larger. Different from the above relationship, the relationship between the hydrolysis rate and the alcohol type is 1-butanol > methanol > ethanol > 2-propanol > 1-propanol, which is from the work of Sadasivan et al. [26]. This

unusual order is caused by two composed factors: the steric hindrance and the polarity of the alcohol. As the molecule weight and chain length in the alcohol increase, the steric hindrance of the solvent increases, resulting in slower diffusion of water molecules in the solvent. Therefore, the hydrolysis and condensation rates are slower. However, as the chain length of the alcohol increases, the polarity of alcohol decreases, which affects the nucleophilic substitution rate. The effect of solvent polarity on the reaction rate depends in part on the relative charge densities of the starting compound and the transition state materials. If the starting material has a higher charge density and if the charges are well dispersed in the transition state, a less polar solvent should lower the energy of the transition state material more than the starting compound. OH^- are small and charge-localized nucleophiles, which have higher charge density than the transition state material $Si(OR)_{4-x}(OH)_x$, so the reduction in solvent polarity will enhance the hydrolysis rate. In other words, alcohols are polar protic solvents, and they have hydroxy groups and will form H-bond with OH^- so that suppresses OH^- to react with TEOS. So, a decrease in H-bonding with OH^- from methanol to butanol will enhance the nucleophilicity of the hydroxide and translate to a higher reaction rate.

3.5 APTES modification of SiO_2 nanospheres

APTES modification is necessary in order to attach Au seeds to SiO_2 as original SiO_2 nanospheres have negative charges [27], which will repel Au seeds. APTES (Fig. 3.9a) is a kind of important aminosilane frequently used in the process of silanization - the functionalization of surfaces with alkoxysilane molecules. Fig. 3.9b shows the reaction of APTES and SiO_2 in an anhydrous environment. The ethoxy groups of APTES molecules

directly react with silanol groups on the surfaces of SiO_2 NPs to form Si-O-Si bonds. After modification, the amino groups provided by APTES attract H^+ ions in solution to become $-NH_3^+$ groups with positive charges. Research from Tan et al. [28] shows the zeta potential of SiO_2 nanospheres after APTES modification was +19.05 mV, which meant that the modified SiO_2 nanospheres had positive charges. Because Au seeds have negative charges, they can attach to SiO_2 nanospheres well.

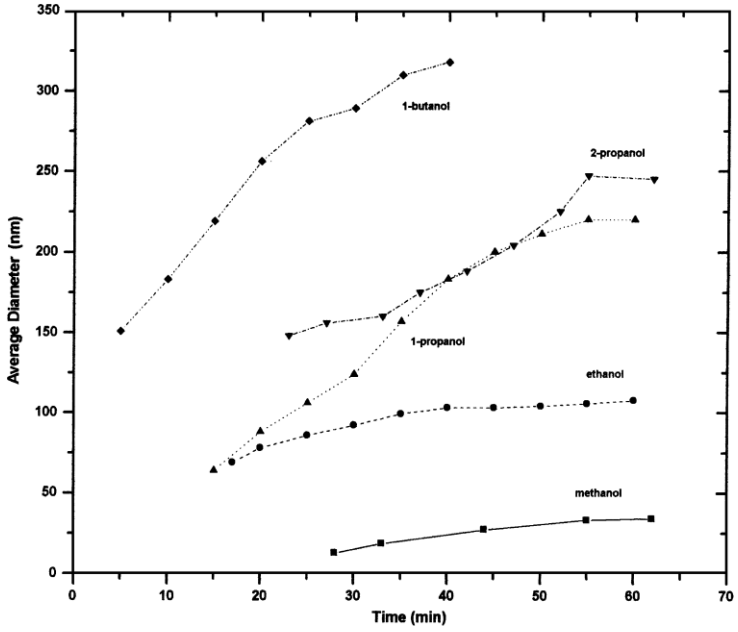

Fig. 3.8 Effect of alcohol type on growth kinetics and size of SiO_2 NPs in different alcohol solutions containing 0.15 mol/L TEOS, 0.5 mol/L NH_3, and 2.5 mol/L H_2O [26].

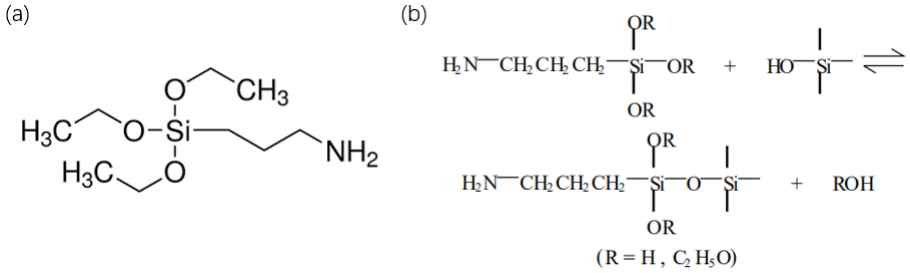

Fig. 3.9 a. Structure of APTES. b. The reaction of APTES modifying SiO_2 in an anhydrous environment.

3.6 PVP modification of SiO_2 nanospheres after gold seeds attachment

After Au seeds were attached, the experimental result in this project showed that the coating of the RF layer directly on the SiO_2 nanospheres failed (Fig. 3.10a). For directly coating RF on SiO_2, it has been known that it cannot be realized from the mixed phase of isolated SiO_2 nanospheres and RF NPs in Fig. 3.10b [29]. Li et al. [27] attributed this phenomenon to the electronic repulsion between the SiO_2 nanospheres and the RF generated from the same charge on their surfaces, which SiO_2 nanospheres synthesized from the Stöber method under alkaline conditions have negative charges on their surfaces. And because the phenol groups in resorcinol are also negatively charged under this pH value, the electrostatic repulsion force between two negatively charged species inhibits adsorption and thus the coating. After APTES modification, the $-NH_3^+$ groups decoration on the SiO_2 surface provides positive charges so that the RF coating process should succeed (Fig. 3.10c). However, Fig. 3.10d shows the result of direct RF coating of SiO_2@APTES synthesized in this project is failed, which indicates the lack of APTES modification on surfaces of SiO_2 nanospheres.

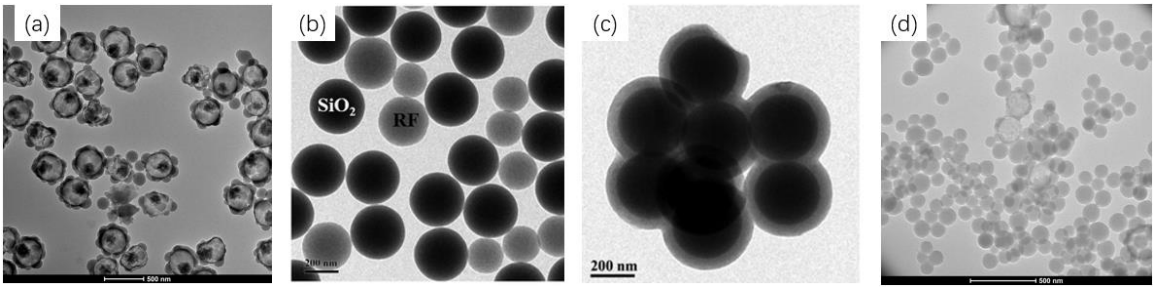

Fig. 3.10 TEM figures of a. failure of direct RF coating after Au seed attachment of SiO_2@APTES in this project; b. RF/SiO_2 composites [29]; c. SiO_2@APTES@RF [29]; d. failure of direct RF coating on SiO_2@APTES in this project.

PVP is a large polymer (Fig. 3.11) that can combine with SiO_2 very well through hydrogen bonding and electrostatic adsorption force between its carbonyl groups and hydroxyl groups on the surface of the SiO_2 nanosphere. The strong hydrogen bonding and electrostatic adsorption force between RF and PVP-modified SiO_2 nanospheres facilitate the RF coating process [30].

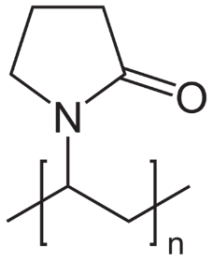

Fig. 3.11 Monomer of PVP molecules.

3.7 RF coating and pre-treatment

RF (resorcinol-formaldehyde) resin is a kind of 3D network structured polymer that is useful in nanostructures. It has high porosities (>80%), surface areas (400-1200 m^2/g), and pore volumes [31]. The synthesis of RF resin includes two steps (Fig. 3.12) [32]. The first step is the addition reaction, which is the reaction of resorcinol (R) and formaldehyde (F) to form hydroxymethyl derivatives ($-CH_2OH$) in the presence of an alkaline catalyst such as Na_2CO_3. The second step is the condensation reaction, in which hydroxymethyl derivatives condense with each other to form a cross-linked wet gel consisting of methylene ($-CH_2-$) and methylene ether ($-CH_2OCH_2-$) bridges nano-sized clusters. After RF coating, use hydrofluoric acid to etch the inner SiO_2 core to create inner spaces for Ag growth: $4HF + SiO_2 \rightarrow SiF_4 \uparrow + 2H_2O$. Using alkali to treat RF to let it have relaxation and Ag^+

can be easier to diffuse through RF later. Egorin et al. [33] explain how an alkaline environment makes the RF layer fluffier: methylol groups and oxymethylene bridges in RF structure are oxidized in an alkaline environment and cause swelling of RF. This treatment makes RF more porous and helps Ag^{+} to diffuse in RF faster [34].

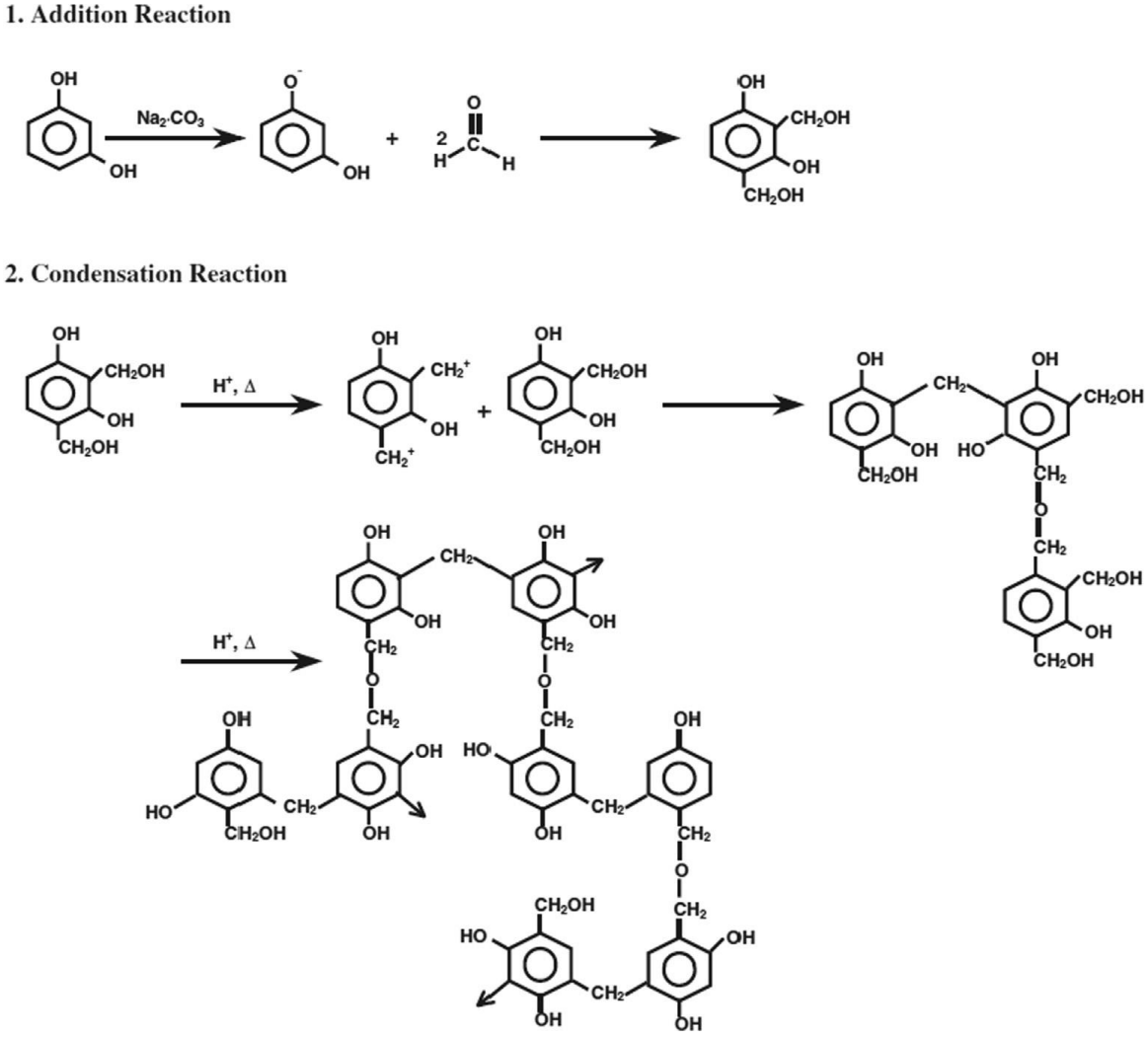

Fig. 3.12 The polymerization reaction of resorcinol with formaldehyde to form RF resin [32].

4 Results

4.1 SiO_2 nanospheres of different sizes

To find the suitable template size, different sizes of SiO_2 nanospheres are synthesized by controlling the volume of $NH_3 \cdot H_2O$ and fixing the volume of TEOS and water (Fig. 4.1).

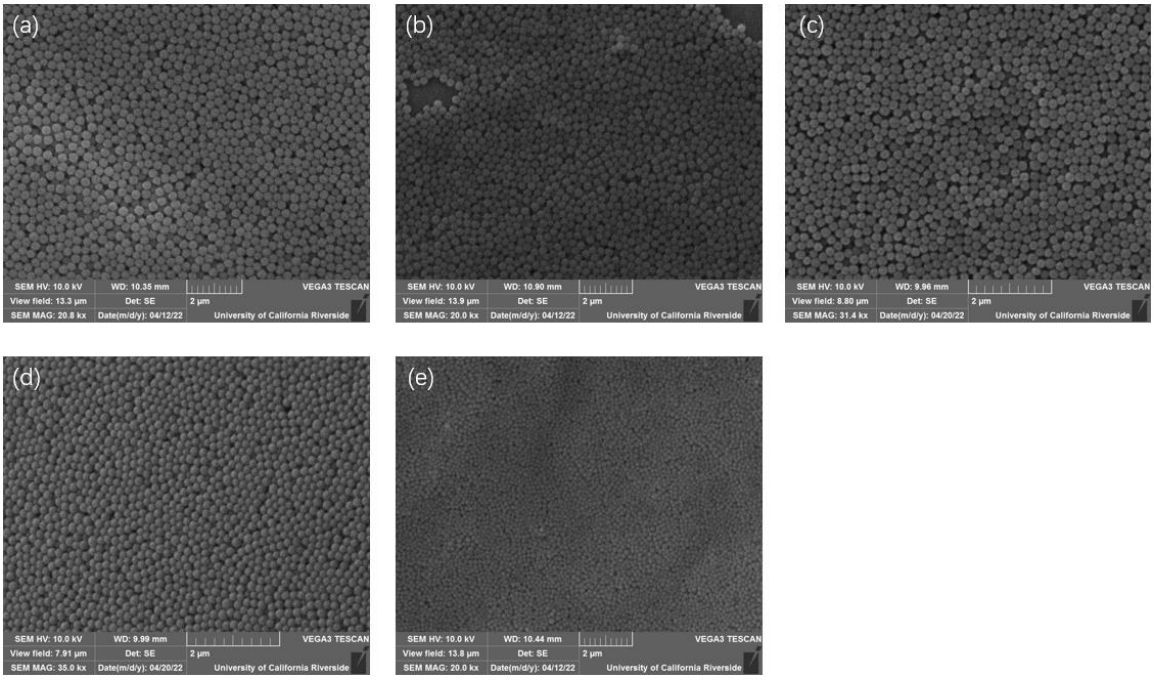

Fig. 4.1 SEM figures of SiO_2 nanospheres synthesized with a. 2.6 mL, b. 1.9 mL, c. 1.7 mL, d. 1.5 mL, and e. 1.3 mL of $NH_3 \cdot H_2O$.

Fig. 4.2a shows the relationship between the volume of $NH_3 \cdot H_2O$ and the average particle size from SEM and DLS. As expected, with a higher volume (concentration) of $NH_3 \cdot H_2O$, the average size of SiO_2 nanospheres is larger, and it is not in a linear relationship. And from DLS measurements, the monodispersity of each group of SiO_2

nanospheres is reasonable and the same as previously mentioned (Fig 3.4 and Fig. 3.5). There is a trend that a higher volume of $NH_3 \cdot H_2O$ brings better monodispersity (Fig. 4.2b).

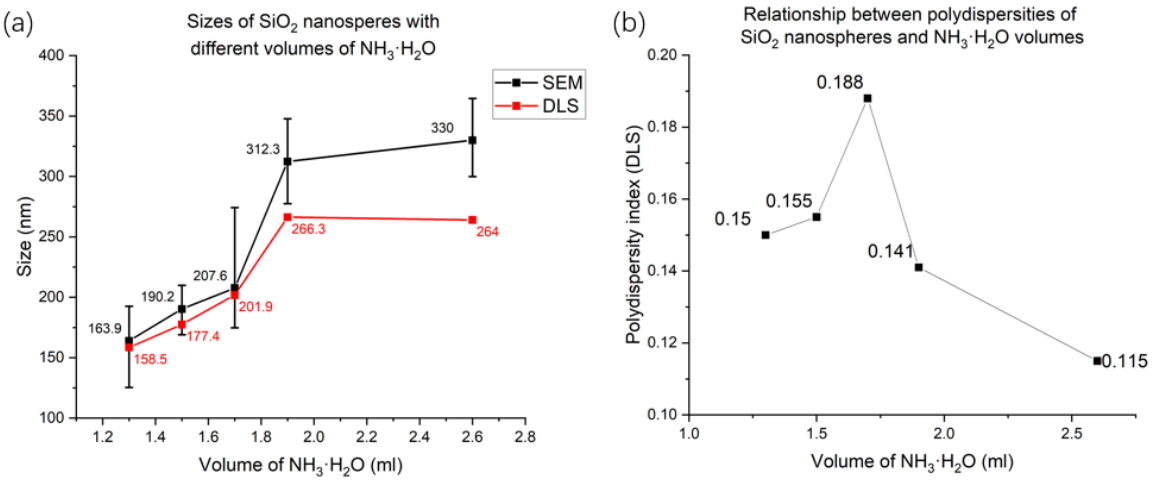

Fig. 4.2 a. Average size and b. polydispersity index of SiO_2 nanospheres synthesized with different volumes of $NH_3 \cdot H_2O$.

4.2 RF shells with different inner sizes before silver growth

Fig. 4.3 shows the TEM figures of RF shell with Au seeds attachment, in which SiO_2 templates are synthesized with 1.3 mL, 1.5 mL, 1.7mL, and 2.6 mL of $NH_3 \cdot H_2O$, and the average sizes of inner spaces are 152.2 nm, 217.6 nm, 236.6 nm, and 327.7 nm (Fig 4.3). Because of the PVP modification, the results of RF coating are very good and Au seeds can attach to the RF shells well. The separation between each RF shell is good and does not have too much connection (the shrink in Fig. 4.3a is because of surface tension caused by the evaporation of ethanol during the TEM sample preparation). In the next growth step, the sample in Fig. 4.3c is used for Ag growth.

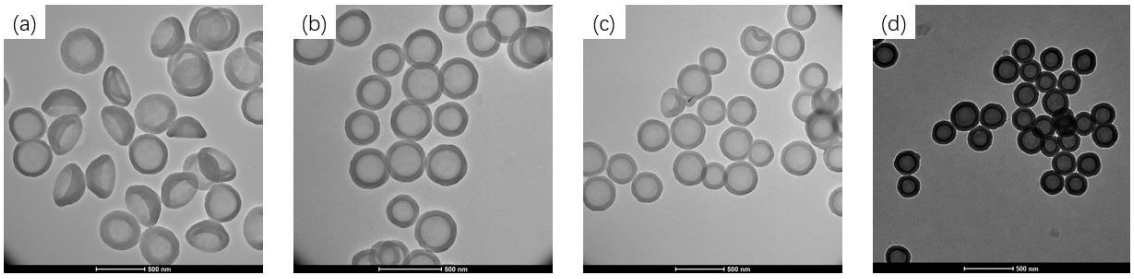

Fig. 4.3 RF shells with Au seeds attached in (a. 2.6 mL b. 1.7 mL c.1.5 mL d. 1.3 mL of $NH_3 \cdot H_2O$ for SiO_2 nanospheres). And the average size of inner spaces in each sample is: a. 327.7 nm, b. 236.6 nm, c. 217.6 nm, and d. 152.2 nm.

4.3 Silver growth in RF shells

Ag^+ precursors of different volumes are injected to discover the relationship between the volume fraction of Ag and the optical properties of Ag@RF NPs. Fig. 4.4a shows the UV-vis absorption spectra of the reaction solution with different volumes of Ag^+ precursor added. As the precursor volume increases, the spectrum becomes broader, and the color of the reaction solution changes from transparent to yellow and then becomes cloudy (Fig. 4.4 b-g) due to the increasing extinction (includes scattering and absorption) of larger Ag NPs.

Fig. 4.5 shows TEM figures of Ag@RF NPs, which are synthesized by adding 100 μl, 300 μl, 500 μl, 700μl and 1100 μl Ag^+ precursor. The average size of inner space and thickness of RF layers are shown in Fig. 4.6. With more Ag^+ precursor added in, the average size of inner spaces of Ag@RF NPs keeps increasing, the RF layers keep thinner, and Ag gradually fills inner spaces. In Fig. 4.5a there are many small Ag NPs outside RF layers, which can be attributed to the reducibility of the RF layer [35] and the slow diffusion of Ag^+ through the RF layer [34]. These small Ag NPs are ripened in later growth. When

1100 µl Ag^+ solution is added, there are several self-nucleated Ag NPs, which may be because the interfacial energy of Ag is not sufficient for nucleation, so it is not easy to grow on the original particles.

In addition, the elasticity of RF shells can also be expressed. With increasing particle size, although the thickness of RF layers decreases, their integrity remains unchanged even though the average internal Ag NPs size has risen to 293.2 nm. The outside shape of the NPs is spherical at the beginning of growth. When the size of Ag is large enough but does not fill the entire inner spaces (Fig 4.5b), the NPs cannot keep spherical temporarily as Ag only grows on existing Au seeds, so they can only press the RF layers from certain directions. However, when Ag fills the entire space, the shape becomes spherical again as RF layers are subjected to the same force in all directions.

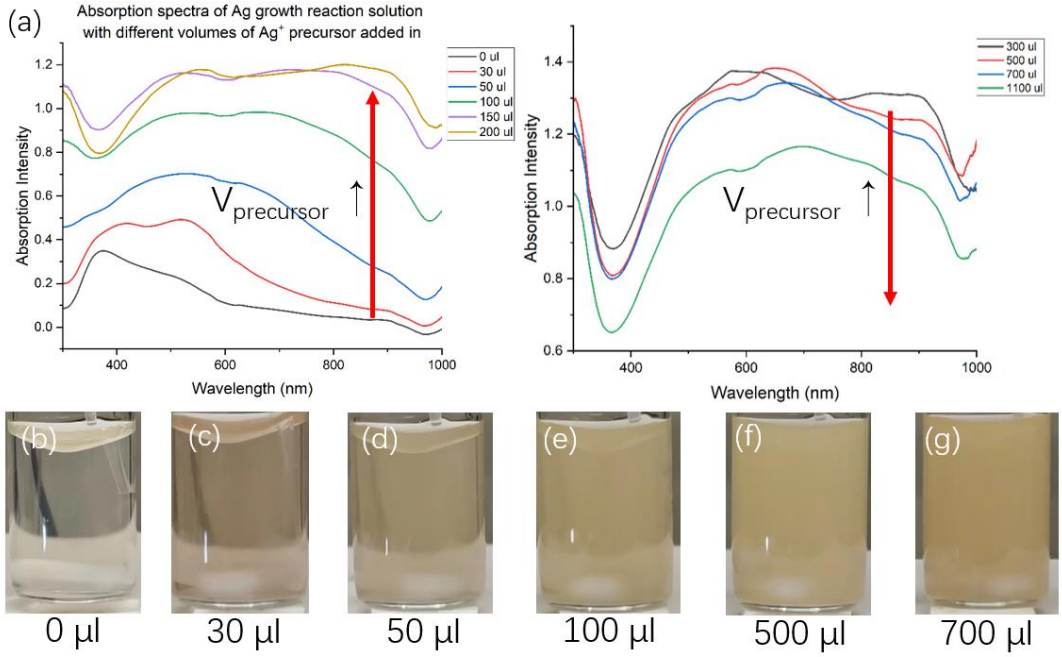

Fig. 4.4 a. Absorption spectrua of the growth solution after adding different volumes of Ag^+ precursor. The color change of reaction solution, which add b. 0 µl, c. 30 µl, d. 50 µl, e. 100 µl, f. 500 µl, g.700 µl Ag^+ precursor.

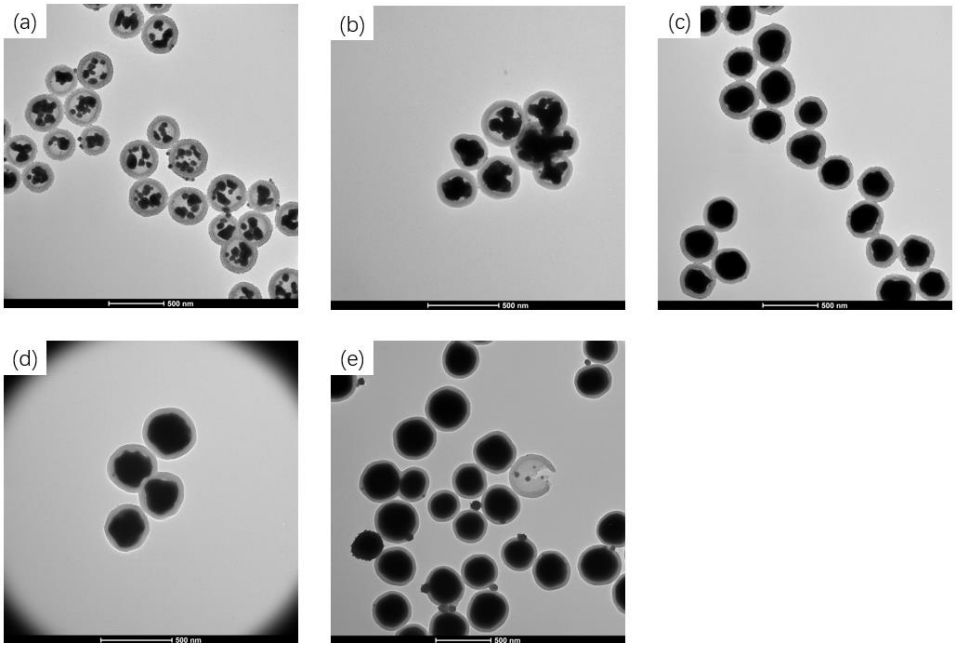

Fig. 4.5 TEM figure of Ag@RF NPs after adding different volumes of Ag^+ precursor: a. 100 µl; b. 300 µl; c. 500 µl; d. 700 µl; e. 1100 µl.

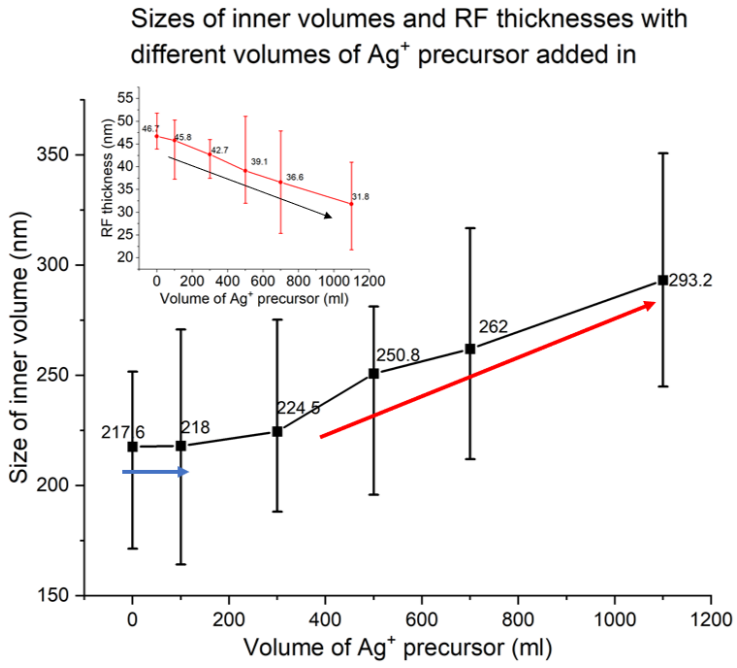

Fig. 4.6 Size of Ag@RF NPs and RF thickness after adding different volumes of Ag^+ precursor.

4.4 Self-assembly of Ag@RF nanoparticles

Fig. 4.7 shows colors of self-assembled photonic Ag@RF crystals under a fluorescent lamp under vertical incidence. It is clear that Ag@RF NPs can self-assemble into photonic crystals. The color changes of samples a to c are the most obvious, which from red to yellow to green, indicating the decrease of reflection wavelength. The reason for the decrease can be briefly described from the generalized equation – Bragg's law [36]: $m\lambda = 2nd\sin(\theta)$, in which m is the diffraction order, λ is the wavelength of incident light that will have diffraction, n is the mean RI of the system composed of colloids and voids, d is the distance between each NP, and θ is angle between incident light and the normal of the plane. As more Ag grows in the RF shells and its low RI compared with that of RF (1.8) and air (around 1 in optical wavelength), the total RI of Ag@RF NPs is lower. As a result, the reflection wavelength has a blueshift. For the green color in sample c, another possible reason is the scattering of green light of large Ag NPs, which is shown in Fig. 1.3.

For samples c to e, the volume fraction difference between Ag and RF does not change much because Ag has filled all inner space, so the RI of Ag@RF NPs does not change too much. However, the size of Ag@RF NPs still increases, making the right part of the equation increase so that the reflection wavelength has a redshift, which may be the reason for the yellow color of sample e.

5 Conclusion

In this project, the feasibility of Ag@RF NPs photonic crystal and relationships between the situation of Ag growth and optical properties of Ag NPs and corresponding

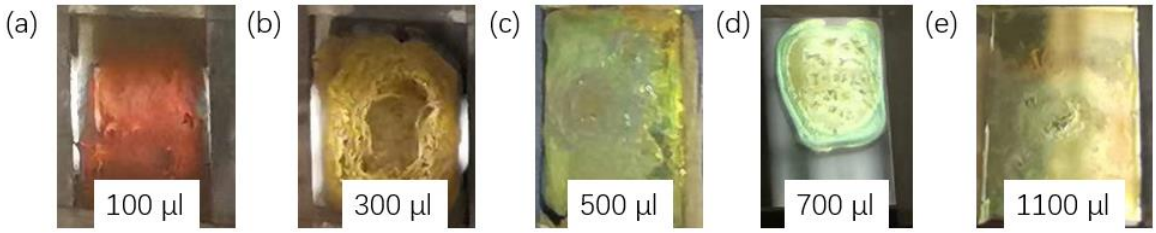

Fig. 4.7 Colors of assembled photonic crystals under vertical irradiation of fluorescent lamp. Ag@RF NPs are synthesized with: a. 100 µl; b. 300 µl; c. 500 µl; d. 700 µl; e. 1100 µl Ag^+ precursor.

self-assembled photonic crystals are investigated. Ag@RF NPs are synthesized by the seeded growth method using relatively uniform hollow RF shells as the templates in which Ag is grown. Increasing the concentration of $NH_3 \cdot H_2O$ can increase the size of SiO_2 nanosphere templates to get larger RF shells. As more Ag grows, the average size of Ag@RF NPs increases, and the RF thickness decreases. Moreover, photonic crystals can be realized by self-assembling Ag@RF NPs in confined areas on glass.

The growth of Ag in RF shells enhances the extinction of Ag@RF NPs. There are obvious changes in reflection wavelengths for different Ag@RF NPs self-assembled photonic crystals due to 1. different RIs of Ag@RF NPs from different Ag volume fractions and size of NPs; 2. the SPR of Ag NPs, which is reflected in higher scattering in green region for larger Ag NPs. As a result, the color of the photonic crystals changes from red to green and then to yellow as more Ag grows.

But this project still needs improvement. To enhance the performance of Ag@RF NPs photonic crystals, the size of SiO_2 templates should be more uniform and the Ag growth should be slower to obtain more uniform Ag@RF NPs. Furthermore, due to the time limit, the complex relationship between the Ag volume fraction and the reflection

wavelength has not been investigated and the exact reflection wavelength of each sample has not been measured by reflection spectroscopy.

Bibliography

[1] Kelly, K. L., Coronado, E., Zhao, L. L., & Schatz, G. C. (2003). The optical properties of metal nanoparticles: The influence of size, shape, and dielectric environment. *ChemInform, 34(16)*. https://doi.org/10.1002/chin.200316243

[2] Mandelbaum, Y., Mottes, R., Zalevsky, Z., Zitoun, D., & Karsenty, A. (2021). Investigations of shape, material and excitation wavelength effects on field enhancement in SERS Advanced Tips. *Nanomaterials, 11(1),* 237. https://doi.org/10.3390/nano11010237

[3] Bolarinwa, H. S., Onuu, M. U., Fasasi, A. Y., Alayande, S. O., Animasahun, L. O., Abdulsalami, I. O., Fadodun, O. G., & Egunjobi, I. A. (2017). Determination of optical parameters of zinc oxide nanofibre deposited by electrospinning technique. *Journal of Taibah University for Science, 11(6),* 1245–1258. https://doi.org/10.1016/j.jtusci.2017.01.004

[4] Khlebtsov, B. N., Khanadeev, V. A., & Khlebtsov, N. G. (2008). Determination of the size, concentration, and refractive index of silica nanoparticles from turbidity spectra. *Langmuir, 24(16),* 8964–8970. https://doi.org/10.1021/la8010053

[5] Paramelle, D., Sadovoy, A., Gorelik, S., Free, P., Hobley, J., & Fernig, D. G. (2014). A rapid method to estimate the concentration of citrate capped silver nanoparticles from UV-visible light spectra. *The Analyst, 139(19),* 4855. https://doi.org/10.1039/c4an00978a

[6] Evanoff, D. D., & Chumanov, G. (2004). Size-controlled synthesis of nanoparticles. 2. measurement of extinction, scattering, and absorption cross sections. *The Journal of Physical Chemistry B, 108(37),* 13957–13962. https://doi.org/10.1021/jp0475640

[7] Rycenga, M., Cobley, C. M., Zeng, J., Li, W., Moran, C. H., Zhang, Q., Qin, D., & Xia, Y. (2011). Controlling the synthesis and assembly of silver nanostructures for Plasmonic Applications. *Chemical Reviews, 111(6),* 3669–3712. https://doi.org/10.1021/cr100275d

[8] Bora, T. (2018). Recent developments on metal nanoparticles for SERS applications. Noble and Precious Metals - Properties, Nanoscale Effects and Applications. https://doi.org/10.5772/intechopen.71573

[9] Langer, J., Jimenez de Aberasturi, D., Aizpurua, J., Alvarez-Puebla, R. A., Auguié, B., Baumberg, J. J., Bazan, G. C., Bell, S. E., Boisen, A., Brolo, A. G., Choo, J., Cialla-May, D., Deckert, V., Fabris, L., Faulds, K., García de Abajo, F. J., Goodacre, R., Graham, D., Haes, A. J., … Liz-Marzán, L. M. (2019). Present and future of

surface-enhanced Raman scattering. *ACS Nano, 14(1)*, 28–117. https://doi.org/10.1021/acsnano.9b04224

[10] Zhong, F., Wu, Z., Guo, J., & Jia, D. (2018). Porous silicon photonic crystals coated with ag nanoparticles as efficient substrates for detecting trace explosives using SERS. *Nanomaterials, 8(11)*, 872. https://doi.org/10.3390/nano8110872

[11] Hassan, M. M., Zareef, M., Jiao, T., Liu, S., Xu, Y., Viswadevarayalu, A., Li, H., & Chen, Q. (2021). Signal optimized rough silver nanoparticle for Rapid Sers Sensing of pesticide residues in tea. *Food Chemistry, 338*, 127796. https://doi.org/10.1016/j.foodchem.2020.127796

[12] Yu, B., Zhai, F., Cong, H., & Yang, D. (2016). Photosensitive polystyrene/silver bromide hybrid colloidal crystals as recoverable colorimetric naked eye probes for bromine gas sensing. *Journal of Materials Chemistry C, 4(7)*, 1386–1391. https://doi.org/10.1039/c5tc02616d

[13] Aluicio-Sarduy, E., Callegari, S., Figueroa del Valle, D. G., Desii, A., Kriegel, I., & Scotognella, F. (2016). Electric field induced structural colour tuning of a silver/titanium dioxide nanoparticle one-dimensional photonic crystal. *Beilstein Journal of Nanotechnology, 7*, 1404–1410. https://doi.org/10.3762/bjnano.7.131

[14] Zhang, L. (2013). Self-assembly Ag nanoparticle monolayer film as SERS substrate for pesticide detection. *Applied Surface Science, 270*, 292–294. https://doi.org/10.1016/j.apsusc.2013.01.014

[15] Gao, C., Goebl, J., & Yin, Y. (2013). Seeded growth route to noble metal nanostructures. *Journal of Materials Chemistry C, 1(25)*, 3898. https://doi.org/10.1039/c3tc30365a

[16] Chen, J., Feng, J., Li, Z., Xu, P., Wang, X., Yin, W., Wang, M., Ge, X., & Yin, Y. (2018). Space-confined seeded growth of black silver nanostructures for solar steam generation. *Nano Letters, 19(1)*, 400–407. https://doi.org/10.1021/acs.nanolett.8b04157

[17] Ghimire, P. P., & Jaroniec, M. (2021). Renaissance of stöber method for synthesis of colloidal particles: New developments and opportunities. *Journal of Colloid and Interface Science, 584*, 838–865. https://doi.org/10.1016/j.jcis.2020.10.014

[18] LaMer, V. K., & Dinegar, R. H. (1950). Theory, production and mechanism of formation of monodispersed hydrosols. *Journal of the American Chemical Society, 72(11)*, 4847–4854. https://doi.org/10.1021/ja01167a001

[19] Han, Y., Lu, Z., Teng, Z., Liang, J., Guo, Z., Wang, D., Han, M.-Y., & Yang, W. (2017). Unraveling the growth mechanism of silica particles in the Stöber method: In situ seeded growth model. *Langmuir, 33(23)*, 5879–5890. https://doi.org/10.1021/acs.langmuir.7b01140

[20] Wang, X.-D., Shen, Z.-X., Sang, T., Cheng, X.-B., Li, M.-F., Chen, L.-Y., & Wang, Z.-S. (2010). Preparation of spherical silica particles by st?ber process with high concentration of tetra-ethyl-orthosilicate. *Journal of Colloid and Interface Science, 341(1)*, 23–29. https://doi.org/10.1016/j.jcis.2009.09.018

[21] van Blaaderen, A., & Kentgens, A. P. M. (1992). Particle morphology and chemical microstructure of colloidal silica spheres made from alkoxysilanes. *Journal of Non-Crystalline Solids, 149(3)*, 161–178. https://doi.org/10.1016/0022-3093(92)90064-q

[22] Yan, Y., Fu, J., Xu, L., Wang, T., & Lu, X. (2016). Controllable synthesis of SiO_2 nanoparticles: Effects of ammonia and tetraethyl orthosilicate concentration. *Micro & Nano Letters, 11(12)*, 885–889. https://doi.org/10.1049/mnl.2016.0434

[23] Lee, K., Sathyagal, A. N., & McCormick, A. V. (1998). A closer look at an aggregation model of the stöber process. *Colloids and Surfaces A: Physicochemical and Engineering Aspects, 144(1-3)*, 115–125. https://doi.org/10.1016/s0927-7757(98)00566-4

[24] Park, S. K., Kim, K. D., & Kim, H. T. (2002). Preparation of silica nanoparticles: Determination of the optimal synthesis conditions for small and uniform particles. *Colloids and Surfaces A: Physicochemical and Engineering Aspects, 197(1-3)*, 7–17. https://doi.org/10.1016/s0927-7757(01)00683-5

[25] Bari, A. H., Jundale, R. B., & Kulkarni, A. A. (2020). Understanding the role of solvent properties on reaction kinetics for synthesis of silica nanoparticles. *Chemical Engineering Journal, 398*, 125427. https://doi.org/10.1016/j.cej.2020.125427

[26] Sadasivan, S., Dubey, A. K., Li, Y., & Rasmussen, D. H. (1998). Alcoholic solvent effect on silica synthesis—NMR and DLS investigation. *Journal of Sol-Gel Science and Technology, 12(1)*, 5–14. https://doi.org/10.1023/a:1008659708390

[27] Li, N., Zhang, Q., Liu, J., Joo, J., Lee, A., Gan, Y., & Yin, Y. (2013). Sol–gel coating of inorganic nanostructures with resorcinol–formaldehyde resin. *Chemical Communications, 49(45)*, 5135. https://doi.org/10.1039/c3cc41456f

[28] Tan, Y., Ding, S., Wang, Y., Jing, A., & Qian, W. (2006). Regenerating optical properties of individual gold nanoparticles in alcoholic solvents without any surfactant. *Journal of Nanoscience and Nanotechnology, 6(1)*, 262–264. https://doi.org/10.1166/jnn.2006.17942

[29] Wang, X., Li, S., Yang, G., Jin, C., & Huang, S. (2020). Insights into the resorcinol–formaldehyde resin coating process focusing on surface modification of colloidal SiO_2 particles. *Langmuir, 36(10),* 2654–2662. https://doi.org/10.1021/acs.langmuir.9b03595

[30] Liu, M., Yu, Y., Liu, B., Liu, L., Lv, H., & Chen, A. (2018). PVP-assisted synthesis of nitrogen-doped hollow carbon spheres for supercapacitors. *Journal of Alloys and Compounds, 768,* 42–48. https://doi.org/10.1016/j.jallcom.2018.07.234

[31] Al-Muhtaseb, S. A., & Ritter, J. A. (2003). Preparation and properties of resorcinol-formaldehyde organic and carbon gels. *Advanced Materials, 15(2), 101–114*. https://doi.org/10.1002/adma.200390020

[32] Wang, H.-L., Hsu, C.-Y., Wu, K. C. W., Lin, Y.-F., & Tsai, D.-H. (2020). Functional nanostructured materials: Aerosol, aerogel, and de novo synthesis to emerging energy and environmental applications. *Advanced Powder Technology, 31(1), 104–120*. https://doi.org/10.1016/j.apt.2019.09.039

[33] Egorin, A. M., Tutov, M. V., Slobodyuk, A. B., & Avramenko, V. A. (2014). Stability of resorcinol-formaldehyde resins in Alkaline Solutions. *Radiochemistry, 56(2),* 183–188. https://doi.org/10.1134/s1066362214020106

[34] Li, Z., Ye, Z., Han, L., Fan, Q., Wu, C., Ding, D., Xin, H. L., Myung, N. V., & Yin, Y. (2020). Polarization-modulated multidirectional photothermal actuators. *Advanced Materials, 33(3),* 2006367. https://doi.org/10.1002/adma.202006367

[35] Chen, L., & Shen, J. (2012). Effect of resorcinol formaldehyde resin gel on the preparation of CO/SiO_2 catalysts for Fischer-Tropsch synthesis. *Chinese Journal of Catalysis*, 33(4-6), 621–628. https://doi.org/10.1016/s1872-2067(11)60342-2

[36] Ge, J., & Yin, Y. (2011). Responsive Photonic Crystals. *Angewandte Chemie International Edition, 50(7),* 1492–1522. https://doi.org/10.1002/anie.200907091